On the thermal properties of knotted block copolymer rings

Neda Abbasi Taklimi[1],[*] Franco Ferrari[1],[†] Marcin Radosław Piątek[1],[‡] and Luca Tubiana[2.3.4§]

[1]*CASA* and Institute of Physics, University of Szczecin, Szczecin, Poland*

[2] *Physics Department, University of Trento,*

Via Sommarive 14, I-38123, Trento, Italy

[3] *INFN-TIFPA, Trento Institute for Fundamental*

Physics and Applications, I-38123 Trento, Italy and

[4] *Faculty of Physics, University of Vienna,*

Boltzmanngasse 5, 1090 Vienna, Austria

(Dated: September 7, 2022)

The thermal properties of coarse grained knotted polymers containing two kinds of monomers A and B fluctuating in a solution are investigated on a simple cubic lattice using the Wang-Landau MC algorithm. These knots have a more complex phase diagram than knots formed by homopolymers, including the possible presence of metastable states. Two different setups are considered: i) charged block copolymers in a ion solution and ii) neutral copolymers with the A monomers above and the B monomers below the theta point. A precise interpretation of the peaks observed in the plots of the specific heat capacity is provided. In view of possible applications in medicine and the construction of intelligent materials, it is also shown that the behavior of copolymer rings can be tuned by changing both their monomer configuration and topology. We find that the most stable compact states are formed by charged copolymers in which very short segments with A monomers are alternated by short segments with B monomers. In such knots the transition from the compact to the expanded state is very fast, leading to a narrow and high peak in the specific heat capacity which appears at very high temperatures. The effects of topology allow to tune the radius of gyration of the knotted polymer ring and to increase or decrease the temperatures at which the observed phase transitions or rearrangements of the system occur. While we observe a general fading out of the influence of topology in longer polymers, our simulations have captured a few exceptions to this rule.

I. INTRODUCTION

Polymer knots are abundant in nature and in artificial polymer materials[1–5]. They can be created in the laboratory[4–6] and have attracted a considerable attention both from experimentalists and theoreticians of several different disciplines including chemistry[7–9], engineering[10], mathematics[11,12] and physics[13–17]. In this work we consider the static properties of knots made by copolymers. We study in particular diblock copolymers consisting of polymers with two different kinds of monomers A and B. Part of the motivations for this work come from biology. In fact, DNA and other biomolecules are characterized by regions that have different properties and can thus be regarded as copolymers. Recently, a diblock copolymer approximation of a piece of DNA has been used in order to understand how the dishomogeneities in the flexibility affect the localization of knots on a piece of circular DNA[18,19]. The study of diblock copolymers can be helpful also in technological applications. For instance, it is already known that the presence of knots affects the behavior of polymer materials. Indeed, the elasticity response of elastomers cannot be understood without considering the fact that the polymer chains inside these materials form knots and links. The effects of the presence of knots in the conformational properties of ring AB diblock-copolymers have already been noted for instance in Ref.[20].

The statistical mechanics of open or circular diblock copolymers has been thouroghly investigated in the past, see e. g.[21–25]. Polyelectrolytes similar to those treated here in Setup I (see below) have been considered in[26]. Setup II has some similarities with the Hydrophilic-Polar (HP) protein model[27], however in our case the B monomers are subjected to attractive forces. The HP model has been studied using the Wang-Landau algorithm in[28,29]. More recently, there has been some interest on circular diblock copolymers with non-trivial topologies[18–20,30–34]. For example, in[33] it has been investigated how the stiffness heterogeneity or the presence of charges influence the localization of the knot. The role of stiffness and heterogeneity in knot production has been explored in Ref.[35]. Other aspects of the topology of diblock-copolymers have been treated in[34]. With the help of the Wang-Landau algorithm[36], the statistical mechanics of knotted diblock copolymers has been studied in Refs.[37–39]. The goal of the present work is to extend the results of[37,39] to longer polymers, showing that remarkable properties emerge in this case. Knotted copolymers are defined here on a simple cubic lattice. Their monomers are subjected to different kinds
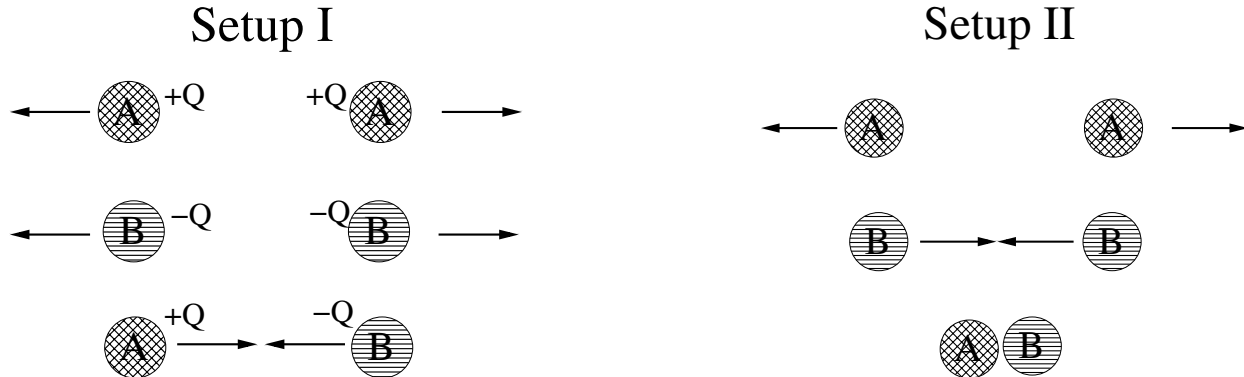
Setup I

Setup II

FIG. 1. This figure summarises the main features of the Setups I and II considered in this paper. Particles in Setup I have a charge Q. Apart from a proportionality factor, we have that $Q \propto \sqrt{\varepsilon}$. The exact value of the proportionality constant is not relevant for performing the calculations. Arrows explain if the interactions are repulsive or attractive. In Setup II the A and B monomers are subjected only to excluded-volume interactions, so that arrows are not necessary in this case.

of very short-range interactions reproducing different physical setups. In one setup, called hereafter Setup I, a charged polymer is fluctuating in an ion solution that screens the long-range Coulomb interactions. Monomers of type A have a positive charge, while monomers of type B are negatively charged. The upshot is that monomers of the same kind repel themselves, while the interactions between the A and B monomers are attractive. Setup I is also relevant for the case of polymers in water. In water at room temperature, in fact, the Bjerrum length l_B amounts to just 7$\mathring{A}$. Let us recall that the constant l_B measures the length scale at which the strength of the Coulomb interactions in a dielectric medium becomes equal to the thermal energy $k_B T$, where k_B is the Boltzmann constant and T is the temperature[40]. In the second studied setup, that will be named Setup II, the solvent is good for the monomers of type A, which thus repel themselves, while monomers of type B are below the theta point and attract themselves. Between monomers of type A and B we suppose that only excluded volume forces are acting. Fig. 1 summarises the main features of both setups. Other setups are possible, see for instance[22].

Multiblock copolymers with different monomer distributions and interactions are considered. We construct knots containing alternating units with n_A monomers of type A and n_B monomers of type B until the total number of monomers N is obtained. If N is not a

multiple of $n_A + n_B$, a slight excess of monomers of type A is allowed. In the following, it will be convenient to introduce the total number N_A of $A-$monomers and the total number N_B of $B-$monomers. Of course $N_A + N_B = N$. Multiblock copolymers of this kind will be denoted with the symbols $M_I(N, n_A, n_B)$ and $M_{II}(N, n_A, n_B)$. The subscripts I and II refer the two setups discussed before. A particularly interesting subcase is that of the $AB-$diblock copolymers composed by two segments, one with A monomers and the other with B monomers. $AB-$diblock copolymers will be distinguished within the more general class of multiblock copolymers introducing the new symbols $D_I(N_A, N_B)$ and $D_{II}(N_A, N_B)$. Of course, $D_{I/II}(N_A, N_B) = M_{I/II}(N, N_A, N_B)$, where I/II means Setup I or II. Following the above conventions, uncharged homopolymer knots with N monomers can be listed under Setup II. A homopolymer knot in a good solvent corresponds to the $AB-$diblock copolymer $D_{II}(N, 0)$ with zero monomers of type B, while a homopolymer knot in a bad solvent can be described with the symbol $D_{II}(0, N)$. To further characterize the analyzed knots, also their monomer composition $f = N_A/(N_A + N_B)$ will be used.

The rationale for investigating knots made by copolymers is to obtain macromolecules with different properties by changing the knot topology, the A/B monomer ratio and the monomer distribution along the chain. We show here that this goal can indeed be achieved and that copolymer knots exhibit a variety of behaviors that are absent in knots formed by homopolymers. In a nutshell, it turns out that the relevant parameters of a polymer ring, like gyration radius, heights and temperatures of the peaks of the heat capacity, specific energy and number of contacts (non-contiguous monomers that are at the distance of one lattice unit, see below for a more precise definition), are highly affected by the monomer distribution. Topology has strong effects on the behaviour of short polymers. In the case of longer polymers, these effects fade out, but still the properties of the knot may be tuned by choosing knots with the same length and monomer distribution, but different topology. Despite the vanishing influence of topology with increasing polymer lengths, we have observed that, in particular cases, the thermal behaviour may drastically change depending on the type of the knot even in longer polymers.

Concluding this Introduction, we would like to stress that the present analysis requires the sampling of knot conformations that are very compact, so that the density of monomers is very high. These compact states often include conformations that are extremely rare and thus very difficult to be sampled using Monte Carlo algorithms. Such conformations may

act as bottlenecks in a Monte Carlo simulation, relevantly increasing the computation time. The problem of handling rare events is not only related to the case of polymer systems. In the Wang-Landau Monte Carlo algorithm, which we will adopt for our simulations, this issue has been already treated in several previous publications, see e. g.[41,42]. Following[43], in this work we have used parallelization techniques to speed up the Wang-Landau algorithm allowing to study the lowest energy conformations. The latter are important because they are dominating at extremely low temperatures. Some of these techniques have been discussed in more details in[44]. In large systems the number of states to be sampled is enormous. In a knot with $N = 500$, for instance, a conformation with the lowest observed energy value can appear once in a set of 10^{11} samples. In the case of a knot with $N = 1000$, the Wang-Landau sampling process requires a few months.

With the inclusion in our calculations of extremely rare configurations, it has been possible to show that the phase diagram of knots formed by block copolymers is more complex than that of homolymers. New peaks appear in the heat capacity corresponding to different transition processes. Particularly interesting is the situation in which most of the monomers are subjected to repulsive interactions apart form a small number of monomers that are able to form contacts with each other. At the lowest temperatures, such knots are found in compact conformations which get soon destroyed upon heating leading to a fast expansion of the knot. With growing temperatures, this expansion continues at a lower pace in Setup I. Finally, at high temperatures these knots behave as their homopolymer counterparts in a good solvent. In some longer knots, metastable compact states have been observed at low temperatures, signalising that knots can be subjected to relevant rearrangements of their structure when heated.

The material presented in this paper is organised as follows. In Section II the used methodology is briefly explained. The obtained results are discussed in Section III. The thermal properties of knots in Setup I and Setup II are presented separately in Subsections III A and III B respectively. Finally, the conclusions and open problems are the subject of Section IV.

II.   METHODOLOGY

Polymer rings are modeled as self avoiding loops on a simple cubic lattice. Monomers are located on the lattice sites and each lattice side can be occupied by at most one monomer. Two consecutive monomers on the loop are linked by one lattice bond, so that the total length of the knot in lattice units is equal to N. The energy of a given knot conformation X is expressed in Setup I and Setup II by the following Hamiltonians respectively:

$$H_I(X) = \varepsilon(m_{AA} + m_{BB} - m_{AB}) \qquad \text{Setup I} \tag{1}$$

and

$$H_{II}(X) = \varepsilon(+m_{AA} - m_{BB}) \qquad \text{Setup II} \tag{2}$$

In Eqs. (1) and (2) the quantities $m_{MM'}$'s count the numbers of contacts between monomers of the kind M and M', where $M, M' = A, B$. Let $\boldsymbol{R}_1, \ldots, \boldsymbol{R}_N$ denote the locations of the N monomers. Two monomers i and j are said to be in contact if $i \neq j \pm 1$ and $|\boldsymbol{R}_i - \boldsymbol{R}_j| = 1$. $\varepsilon > 0$ is an energy scale measuring the cost of one contact, which can be positive or negative depending on the setup and on the monomer types. We note that the Hamiltonian $H_{II}(X)$ of setup II is a variation of the HP protein model[27] with the B monomers being identified with the polar (P) aminoacid residues. The difference is that in setup II we have that the A monomers are repelling themselves due to the short-range interaction $+\varepsilon m_{AA}$, while in the HP model they are only subjected to excluded volume interactions. For convenience, we will introduce the rescaled temperature $\boldsymbol{T} = \frac{k_B T}{\varepsilon}$. To go back from $\boldsymbol{T}$ to the usual temperature T measured in Kelvins some assumptions on ε are needed. For instance, we suppose that the strength ε of the interactions is a multiple of the energy associated with thermal fluctuations at room temperature T_0, i. e. $\varepsilon = q k_B T_0$, where $T_0 \sim 298 K°$ and q is a positive real constant. At this point it is easy to see that the temperature T is expressed in terms of $\boldsymbol{T}$ as follows: $q \boldsymbol{T} T_0 = T$. For example, if $q \sim 1.5$, the point $\boldsymbol{T} = 1$ corresponds to the temperature $T = 1.5 T_0 \sim 447 K°$. After the passage $T \longrightarrow \boldsymbol{T}$, it is possible to eliminate the ε factor in the Hamiltonians of Eqs. (1) and (2). The upshot is that we obtain the following rescaled Hamiltonians: $\boldsymbol{H}_{I,II}(X) = \frac{H_{I,II}(X)}{\varepsilon}$. Here $H_{I,II}$ can be either of the two Hamiltonians defined in Eqs. (1) and (2).

The simulations are performed using the Wang-Landau Monte Carlo algorithm[36]. The initial knot conformations are obtained by elongating the existing conformations of minimal

length knots[45,46] until the desired final length is attained. Knots up to six crossing according to the Rolfsen table are studied, though there is no restriction against including more complicated knots. The details on the sampling and the treatment of the topological constraints can be found in Refs.[47] and[48]. The random transformations that are necessary for sampling the different knot conformations are the pivot moves of Ref.[49]. In order to preserve the topological state of the system, the pivot algorithm and excluded area (PAEA) method of Ref.[47] is applied.

The partition function of the polymer knot is given by:

$$Z(\boldsymbol{T}) = \sum_{E=E_{min}}^{E_{max}} e^{-E/\boldsymbol{T}} g(E) \tag{3}$$

where $g(E)$ denotes the density of states:

$$g(E) = \sum_{X} \delta(\boldsymbol{H}_{I,II}(X) - E) \tag{4}$$

$g(E)$ is the quantity to be evaluated via Monte Carlo methods. E_{min} and E_{max} represent respectively the minimum and maximum values of the energy. The whole energy range $\mathcal{I} = [E_{min}, E_{max}]$ over which the sampling is performed depends on the used setup, the length of the knot, its topology and the selected monomer distribution. To determine the values of E_{min} and E_{max}, a preliminary run without specifying any energy limit is performed. In doing that we exploit the fact that the Wang-Landau algorithm is very efficient in exploring the whole energy range of the system. The preliminary run is stopped when no new values of the energy are found. After that, the averages of the observables are computed by a second run with the values of E_{min} and E_{max} calculated from the preliminary run. Also in this second run the energy range is kept open, but for the convergence of the Wang-Landau algorithm only the energy values in the interval $[E_{min}, E_{max}$ are considered. For the convergence of the Wang-Landau algorithm the sampling of an order of 10^{12} conformations is necessary. If new values of E_{min} and E_{max} appear during the sampling, the run is repeated with the new, extended energy range. In the case of long polymers with $N \geq 300$, cuts in the energy range are necessary in order to obtain the corvergence of the Wang-Landau algorithm in a reasonable time. In this case, several runs are repeated by slightly changing the energy range to check that the results are independent of the energy range despite these small variations. It turn out that the Wang-Landau algorithm is very robust in this sense. For
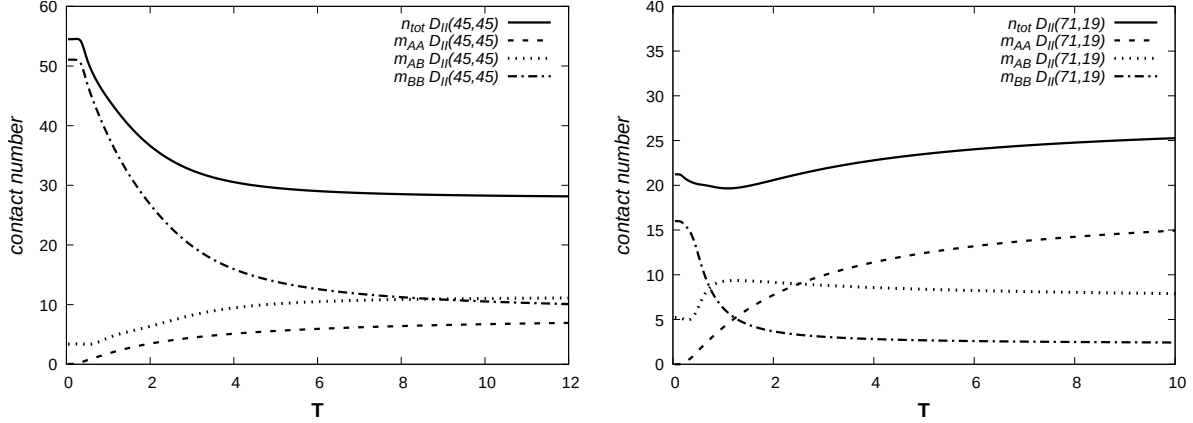
FIG. 2. While the specific energy is relevant for understanding the behavior of homopolymers, in the case of copolymers the numbers of contacts formed by the A and B monomers and the total number of contacts $n_{tot} = m_{AA} + m_{BB} + m_{AB}$ are very useful quantities too. The pictures show how the numbers n_{tot}, m_{AA}, m_{AB} and m_{BB} change with the temperature in the case of a knot 3_1 with monomer distributions $D_{II}(45, 45)$ (left panel) and $D_{II}(71, 19)$ (right panel).

instance, small variations of the energy range do not have relevant influences on the height and the position of the peaks of the specific heat capacity. The averages of the observables are particularly insensitive under changes of E_{max}, while variations of a few percent occur at very low temperatures by changing E_{min} in the case of block copolymers in setup I, which is the most critical with respect to the computational time.

The expectation values of any observable $\mathcal{O}$ may be computed using the formula:

$$\langle \mathcal{O} \rangle(\boldsymbol{T}) = \frac{1}{Z(\boldsymbol{T})} \sum_{E=E_{min}}^{E_{max}} e^{-E/\boldsymbol{T}} g(E) \mathcal{O}_E \tag{5}$$

Here $\mathcal{O}_E$ denotes the average of $\mathcal{O}$ over all sampled states with rescaled energy E. The observables that will be considered in this work are the mean specific energy

$$\frac{\langle E(\boldsymbol{T}) \rangle}{N} = \sum_{E=E_{min}}^{E_{max}} E e^{-E/\boldsymbol{T}} g(E) \tag{6}$$

the specific heat capacity $C/N = \frac{1}{N} \frac{\partial \langle E(\boldsymbol{T}) \rangle}{\partial \boldsymbol{T}}$ and the mean square average of the gyration radius R_G^2. Additional information on the shape of the knot at different temperatures and energies has been gathered studying the number of contacts formed by the monomers and by closed inspection of the generated conformations.
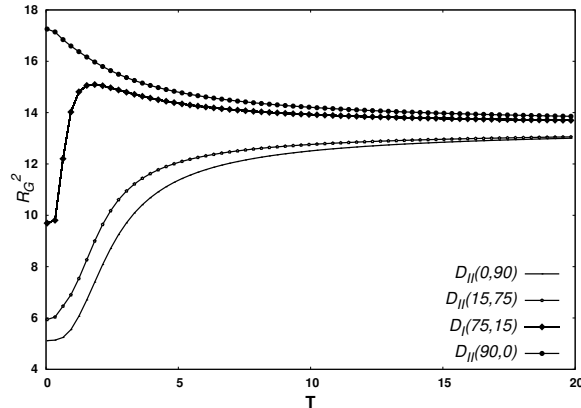
FIG. 3. The gyration radius of the knot 3_1 with $N = 90$ in various monomer distributions is plotted as a function of $\boldsymbol{T}$.

III. THERMAL PROPERTIES OF KNOTTED DIBLOCK COPOLYMER RINGS

Both Setups I and II are characterised by the coexistence of the attractive and repulsive interactions. The monomers of type A or B may attract or repel themselves or the monomers of the other type. In Setup II only the excluded-volume forces are acting between the A and B monomers. In this situation, depending on the temperature, a particular interaction can become more relevant than the others in shaping the behavior of knotted block copolymers and lead to different regimes. The averages of the numbers m_{AA}, m_{BB}, m_{AB} of the contacts formed by the monomers of a specific type with themselves or with the other type together with the averaged total number of contacts $n_{tot} = m_{AA} + m_{BB} + m_{AB}$ provide some hint about the knot's conformations in these regimes. An example of such plots is given in Fig. 2, in which a knot 3_1 in Setup II with different monomer distributions is considered. Another quantity that is important is the specific energy. It turns out that, as it is expected, at any given temperature the specific energy of a copolymer knot never exceeds the specific energy of a homopolymer knot of equal length and topology in a good solvent, where all monomers repel themselves. On the other side, it will always be bigger than that of a homopolymer in bad solvents. A similar trend is observed in the case of the gyration radius as shown in Fig. 3: At any given temperature, the gyration radii of 3_1 knots with different monomer compositions range between a minimum provided by the the gyration radius of the 3_1 homolymer knot $D_{II}(0, 90)$ and an upper limit given by the 3_1 homopolymer knot $D_{II}(90, 0)$. Another
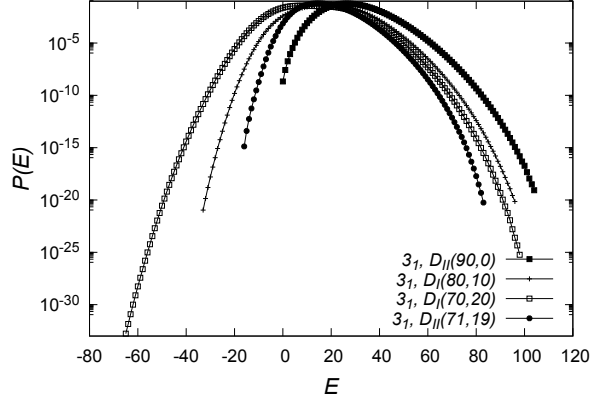
FIG. 4. The probability $P(E)$ of obtaining a state of energy E for a knot 3_1 with $N = 90$ in various monomer distributions is plotted as a function of the energy E.

feature which is visible in Fig. 3 is that the swelling process under increasing temperatures may become much more rapid when the knot contains monomers of different kinds. For example, the gyration radius of the knot 3_1 with monomer distribution $D_I(75, 15)$ changes faster than that of the homopolymer $D_{II}(0, 90)$ and the diblock copolymer $D_{II}(15, 75)$. We also note that the diblock copolymer $D_I(75, 15)$ exhibits a swelling phase at lower temperatures followed by a mild shrinking phase at higher temperatures. This behavior becomes stronger with growing topological complexity. In the following, we will discuss the results obtained for knots in Setup I and Setup II separately.

To conclude the discussion on the general features of knots formed by copolymers, we stress that the Monte Carlo sampling is much more difficult for knots in Setup I than in Setup II. The reason can be understood by looking at Fig. 4 where the probability $P(E)$ of states of energy E has been computed for a few knots in both setups. That figure shows that knots admit in Setup I conformations in the lowest part of the energy spectrum that are much more rare than any knot conformation in Setup II. This makes the sampling of the lowest energy states in Setup I very difficult, especially for long knots. Of course, the energy spectrum, and thus also the existence of rare ultralow energy conformations, strongly depends on the monomer composition of a knot. This is visible by looking in Fig. 4 at the differences between the same knot 3_1 with $N = 90$ in the monomer distributions $D_I(80, 10)$ and $D_I(70, 20)$. However, even in the case in which the monomer distribution is fixed, the energy range grows considerably when passing from Setup I to Setup II. For example, the
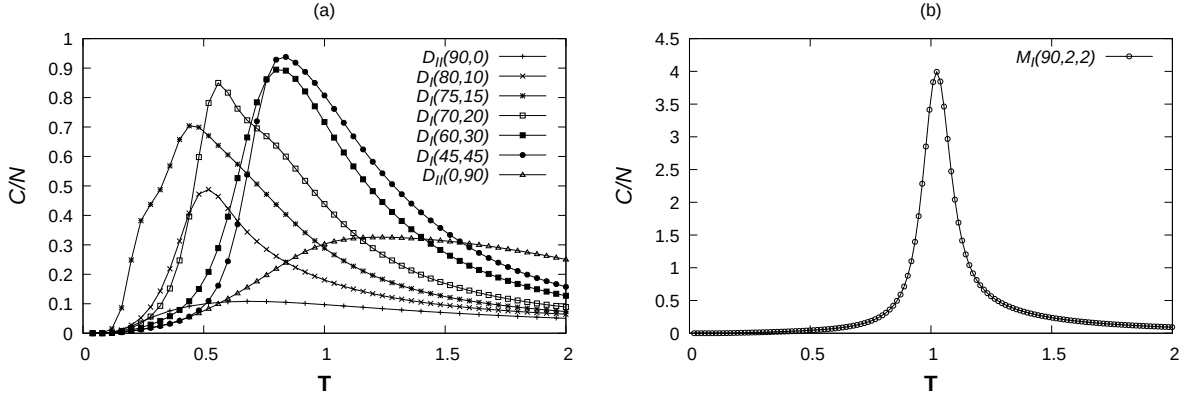
FIG. 5. The specific heat capacity C/N of a knot 3_1 with $N = 90$ in various monomer distributins is plotted as a function of T. The peak of C/N is highest in the case of the monomer distribution $M_I(90, 2, 2)$ (panel b) and lowest in the case of the homopolymer $D_{II}(90, 0)$ (plot with crosses at the bottom of the picture in panel a).

most compact state of a 3_1 knot with $N = 90$ and monomer distribution $D_I(70, 20)$ has an energy $E < -60$ and a probability that is below 10^{-30}. In the same knot 3_1 with $N = 90$ and the similar monomer distribution $D_{II}(71, 19)$, the probability of the lowest energy state is higher of more than 15 orders. In a knot 4_1 with $N = 1000$ with monomer distribution $D_I(800, 200)$ the lowest energy state has a probability lower than 10^{-256}.

A.   Results for Setup I

The variety of behaviors that it is possible to obtain in the case of short copolymer knots is shown in Figs. 5 and 6[56]. Both figures refer to the same trefoil knot 3_1 of length $N = 90$. In Fig. 5 the range of temperatures has been restricted to the interval $0.00 \leq T \leq 2.00$ in order to display in details the features of the peaks of the specific heat capacity C/N. The different plots of the specific heat capacity and the mean square gyration radius R_G^2 have been obtained only by varying the distribution of the A and B monomers. It is possible to realize from Fig. 5 that the heights of the peaks of the specific heat capacity and the temperatures at which this peak occurs are very sensitive to the momomer distribution. The peaks' heights range in fact from about 0.11 for the homopolymer $D_{II}(90, 0)$ (see plot with crosses at the bottom of Fig. 5, panel a, and comments in the caption) up to about

TABLE I. In the second column of this table are reported the values of the height of the peaks of the specific heat capacity for a knot 3_1 with different monomer distributions. In the third column it is shown the temperature $\boldsymbol{T}_{MAX}$, at which the heat capacity is at its maximum. The plots of the specific heat capacity are displayed in Fig. 5.

Monomer distribution	Peak height	Temperature $\boldsymbol{T}_{MAX}$
$D_{II}(0,90)$	0.33	1.22
$M_I(2,2)$	3.99	1.03
$D_I(45,45)$	0.87	0.94
$D_I(60,30)$	0.72	0.94
$D_{II}(90,0)$	0.11	0.69
$D_I(70,20)$	0.85	0.56
$D_I(80,10)$	0.49	0.51
$D_I(75,15)$	0.70	0.48

4.00 in the case of the multiblock copolymer $M_I(90,2,2)$ in Fig. 5, panel b. In general, we observe that the swelling process when the temperature increases is much more abrupt in knots with monomer distributions $M_I(N,2,2)$ than in those with any other monomer distribution. Consequently, the specific heat capacities in knots with monomer distribution $M_I(N,2,2)$ are characterised by high and narrow peaks as it can be seen by comparing the plot of C/N in Fig. 5, panel b for the distribution $M_I(90,2,2)$ with the plots of the other distributions in panel a. By gradually increasing the size of the basic unit in the multiblock copolymer, for instance choosing $M_I(90,4,4)$, $M_I(90,8,8)$ etc., the peak of the heat capacity becomes gradually lower and wider. We also note that the temperature at which the peak of the specific heat appears can be fine-tuned by choosing the monomer distribution. The temperatures and the height of the peaks related to different distributions are displayed in Table I. The data in the table are ordered according to decreasing temperatures $\boldsymbol{T}_{MAX}$, whose values range in the wide interval $0.48 \leq \boldsymbol{T}_{max} \leq 1.22$.

The distribution of the A and B monomers greatly influences also the allowed range of possible sizes as shown in Fig. 6. For example, in the 3_1 copolymer knot in the setup
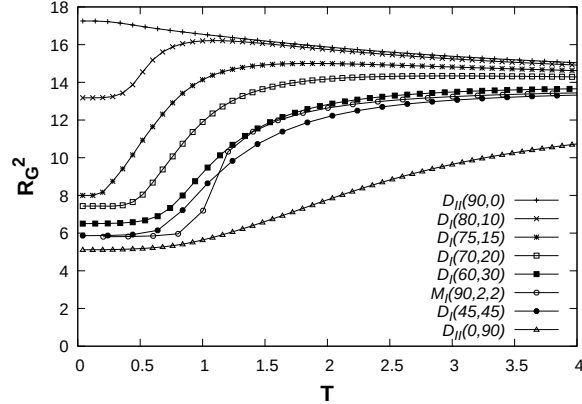
FIG. 6. The mean square gyration radii R_G^2 of a knot 3_1 with $N = 90$ in various monomer configurations is plotted as a function of $\boldsymbol{T}$. Going from the top to the bottom it is possible to distinguish the plots of the gyration radii for the following monomer distributions: $D_{II}(90, 0)$, $D_I(80, 10)$, $D_I(75, 15)$ and $D_I(70, 20)$. Below, there is a partial overlapping of the plots of the mean square gyration radii for the distributions $D_I(60, 30)$ (line with black squares), $M_I(90, 2, 2)$ (line with white circles) and $D_I(45, 45)$ (line with black circles). The plot in the bottom part of the figure is that of the homopolymer in a bad solvent $D_{II}(0, 90)$ (white triangles).

$D_I(80, 10)$ the values of the mean square gyration radius are restricted to the narrow interval $13 \le R_G^2 \le 16$. By passing to the $D_I(75, 15)$ distribution, a change that requires just the substitution of five monomers of type A with monomers of type B, the new range in which R_G^2 can take its values is $8.86 \le R_G^2 \le 14.89$. Thus even little variations in the monomer distribution are able to introduce significant changes in the expectation values of the gyration radius. Let us note that all gyration radii in Fig. 6 converge to a common limit at very high temperatures as it is expected, because at high temperatures the interactions between the monomers are no longer relevant due to the strong thermal fluctuations. From Fig. 6 it turns also out that, as expected, at any temperature the self-attracting homopolymer 3_1 knot $D_{II}(0, 90)$ is always much smaller than all other trefoil knots in which repulsive interactions are present.

One goal of this work is to investigate how the topology of a knot influences its thermal behavior. In the case of homopolymers it is known that the topological effects are particularly strong in short knots and gradually fade out with increasing length, see e. g.[48]. This is true also in the case of copolymers. The plots in Fig. 7 show the gyration radii of a few
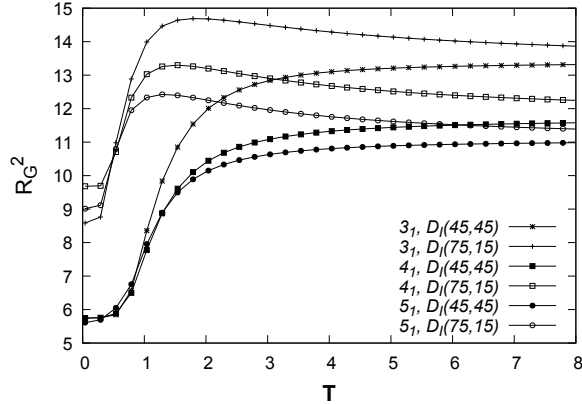
FIG. 7. Presented are the plots of R_G^2 in the case of the knots $3_1, 4_1$ and 5_1 with $N = 90$. For each knot two values of f are considered: $f = 0.50$, corresponding to the monomer distribution $D_I(45, 45)$ and $f \sim 0.83$, corresponding to the monomer distribution $D_I(75, 15)$.

$AB-$diblock copolymers of knot types $3_1, 4_1$ and 5_1. For each knot type two different monomer distributions have been taken into account, namely $D_I(45, 45)$ and $D_I(75, 15)$. Fixing the monomer distribution and the knot length, which is equal to $N = 90$, we expect the differences in the plots to be due to pure topological effects. The latter are quite evident in the figure. For instance, by looking at the gyration radii of the knots with monomer distribution $D_I(45, 45)$, it is clear that the sizes of these knots are changing with the topology. The same conclusion is valid if we look at the plots with monomer distribution $D_I(75, 15)$. It should be noticed that topological effects are less marked than those connected with the modification of the monomer distribution. This fact is well illustrated also by the plots of the specific heat capacity. Fig. 8 shows that by changing the topology of a knot while keeping its monomer distribution fixed, it is possible to shift significantly the peaks of the specific heat capacity but to a smaller extent than in the case in which the topology is fixed and the monomer distribution is modified.

The above comments concerning the topological effects are valid also in the case of longer polymers. The plots in Figs. 9 and 10 of the gyration radius and heat capacity respectively illustrate the influence of both topology and monomer distribution on the thermal behaviour of various knots of length $N = 200$. Fig. 9 shows that topology is affecting the knot size. Moreover, the shape of the peaks of the specific heat capacity changes with the topology of the knot, as it is possible to see in Fig. 10. These changes cannot be attributed to
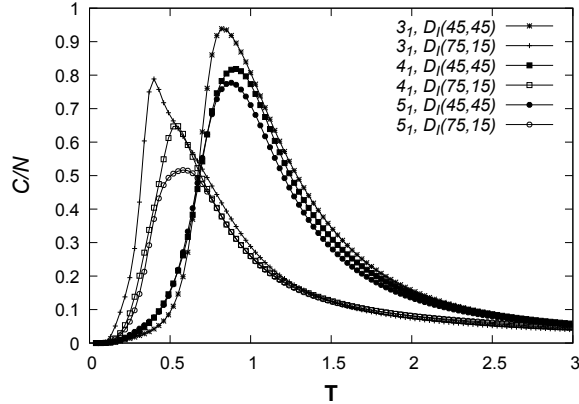
FIG. 8. Dependence of the specific heat capacity C/N on the topology and on the monomer composition f for $AB-$diblock copolymers. Presented are the plots of C/N in the case of the knots $3_1, 4_1$ and 5_1 with $N = 90$. For each knots two values of f are considered: $f = 0.50$ (case $D_I(45, 45)$) and $f \sim 0.83$ (case $D_I(75, 15)$).

statistical errors, as it has been verified by repeating the simulations starting from different seeds. Of course, with increasing polymer lengths the topological effects start to fade out. In particular, the range of temperature in which the peaks of the specific heat capacity are appearing is approximately the same independently of topology for all knots considered in Fig. 10. This is not the case of the shorter knots with $N = 90$, see Fig. 8.

The novelty when $N = 200$ with respect to shorter polymers is the appearance of double peaks or of a peak with a shoulder in the specific heat capacities of the knots with monomer distribution $D_I(167, 33)$, see Fig. 10. A double peak is characterising also the specific heat capacity of the knots 0_1 and 6_1 with $N = 200$ and monomer distribution $D_I(167, 33)$ (not shown in the figure). This phenomenon is accompanied by a pattern that is visible in the behaviour of the mean square gyration radius R_G^2 at low temperatures. An example of this behaviour is shown in the inset of Fig. 9, in which the plot of R_G^2 of a knot 4_1 with monomer distribution $D_I(167, 33)$ is displayed in greater detail. As it is possible to see, there is a rapid increase of R_G^2 in the range of temperatures $0.4 \leq \boldsymbol{T} \leq 0.6$. This range coincides approximately with that in which the peak of the specific heat capacity of the knot 4_1 centered at about $\boldsymbol{T} = 0.50$ is appearing, see the line with empty squares in Fig. 10.

The appearance of double peaks and peaks with shoulders in the plots of the heat capacity of chains has been shown to be related to the occurrence of two different phase transitions

in a small interval of temperatures, see[50–53] and[26] in the case of polyelectrolytes. To understand what happens in the present context, we recall the behaviour of homopolymers upon heating. In homopolymers in a good solvent all monomers are subjected to purely repulsive interactions. At the lowest temperatures, the number of contacts between the monomers is minimal and the knot attains its maximally swollen size. When the temperature is rising, the increasingly strong thermal fluctuations become energetic enough to break the potential barrier that prevents the formation of contacts between the monomers. As a consequence, the size of the knot moderately shrinks with growing temperatures. This shrinking is moderate and the related process causes just a small peak in the heat capacity, see the examples of Fig. 10, right panel. In homopolymers in a bad solvent, on the contrary, the minimal size conformations are found when the temperature is very low. The compact states that arise in this case consist of a large number of contacts. With growing temperatures, the number of contacts decreases and the knot continues to swell up to high temperatures until the thermal fluctuations dominate over the interactions. At this point, the gyration radius and the number of contacts of the ring are completely determined by entropy and the knot's topology. This swelling process in a bad solvent generates in the plots of the specific heat capacity a broad peak extending over a large interval of temperatures.

In block copolymers, the situation is different because there are simultaneously both attractive and repulsive interactions. Knotted diblock copolymers with $N_A \sim N_B$ have a behaviour similar to that of knotted homopolymers in a bad solvent. The reason is that, when $N_A \sim N_B$, the attractive forces are very strong because there is a large number of A and B monomers that may build contacts with each other. As a consequence, for energy reasons, at very low temperatures the number of contacts between the A and B monomers is at its maximum and the volume occupied in space by the knot is very small, though not so small as in the homopolymer case. With growing temperatures, similarly to what happens for knotted homopolymers in a bad solvent, the number of contacts decreases and the swelling process continues also when the temperature is high. In knots of length $N = 90$ and $N = 200$ the expansion is completed at a temperature of $\boldsymbol{T} \sim 3$ when $N_A = N_B$. The result is a broad peak in the specific heat capacity with the maximum of the peak at a temperature of $\boldsymbol{T} \sim 1$ (see Figs. 8 and 10) or higher like in the case of the knot 5_1 with length $N = 500$ and monomer distribution $D_I(250, 250)$ of Fig. 14. A thorough investigation with a knot 4_1 of length $N = 200$ has shown that the behaviour of knots with $N_A \sim N_B$

described before still persists at least until $N_A = 150$ and $N_B = 50$. This means that the heat capacity is characterised only by a single peak. Of course, the heights of this peak will decrease with decreasing values of N_B because less and less contacts between the A and B monomers are possible.

Below a certain threshold of the number N_B of available B monomers, knots depart significantly from the behaviour described above. To fix the ideas, we will say that such knots have monomer configurations of the type $N_A >> N_B$. In this case the number of B monomers that are able to form contacts with the A monomers is extremely limited. This explains why the heights of the peaks of the specific heat capacity are decidedly lower than those of knots in which the monomer distribution is $N_A \sim N_B$, see Fig. 10. Despite the fact that $N_B << N_A$, at very low temperatures the number of contacts m_{AB} between the monomers of types A and B is quite high in order to minimise the energy according to the Hamiltonian (1). Indeed, a knot 4_1 with $N = 200$ and monomer distribution $D_I(167, 33)$ has been studied in details in order to understand the origin of the double peak when $N_A >> N_B$. It turns out that at the minimum energy value $E_{min} = -111$, the average total number of contacts formed by this knot is $\langle n_{tot} \rangle = 122$. The overwhelming majority of these contacts is due to the A and B monomers, because at $\boldsymbol{T} \sim 0$ we have that $\langle m_{AB} \sim 118$, $\langle m_{AA} \rangle \sim 4$ and $\langle m_{BB} \rangle = 0$. Of course, with rising temperatures m_{AB} will decrease similarly as in the case $N_A \sim N_B$ illustrated before. The striking difference between the cases $N_A \sim N_B$ and $N_A >> N_B$ is however that knots with $N_A >> N_B$ undergo an extra rearrangement of their structures at very low temperatures. More precisely, knots with $N_A >> N_B$ are approaching a very compact state when the temperature becomes very low like their counterparts with $N_A \sim N_B$. In the case of the prototype knot 4_1 mentioned above, this state contains $\langle m_{AB} \rangle \sim 103$ contacts between the A and B monomers. The breaking of these contacts causes a swelling process that produces in the plot of the specific heat capacity a peak around the temperature $\boldsymbol{T} \sim 0.7$, see Fig. 10, left panel, plot with white circles. This is the origin of the second peak in the heat capacities of the knots with monomer distribution $D_I(167, 33)$ in Fig. 10. When the temperature further decreases, the quantity R_G^2 of the 4_1 knot changes very rapidly from 30 to 24, see the inset of Fig. 9. This points to the fact that a rearrangement of the structure of the knot has taken place. This rearrangment is connected with the formation of only a small number of new contacts. Unfortunately, the close inspection of very rare conformations at the lowest energies is very difficult, but it has

been possible to capture conformations at the energies $E = -105$ and $E = -100$ of the knot 4_1 with $N = 200$ and monomer distribution $D_I(167, 33)$, see Fig. 11. Basing on the available data, our interpretation of the phenomena associated with the presence of the two peaks in the specific heat capacity of knots in which $N_A >> N_B$ is as follows. The second peak, appearing in all observed cases at temperatures $\boldsymbol{T} > 0.5$, is due to the breaking of the contacts that are responsible for a bulk compact state that arises due to the attractive forces between the A and B monomers. The first peak, observed at temperatures $\boldsymbol{T} < 0.5$, is due to a rearrangement of the knot, or at least a part of it, involving the formation of just a few additional contacts. We suspect that the rearrangement is mostly concerning the segment with the A monomers. Above the transition, there is a bulk compact state which is held together by the portion of the A monomers that are in contact with the B monomers. The other A monomers cannot form contacts because of the few B monomers available. As a consequence, these A monomers form a long tail departing from the bulk compact state and fluctuating almost freely. Below thetransition, a rearrangement leading to the formation of additional contacts with more A monomers becomes possible and the tail disappears or is reduced. A close inspection of the conformations of the knot 4_1 that have been captured confirms the above claim, see Fig. 11 and comments in the related captions.

Other rearrangements could become possible in longer polymers. They give rise to metastable states that may appear when the temperature is low, so that the formation of contacts between the A and B monomers is energetically convenient. Such metastable states and also the double peak are not observed in short knots, like for instance those with $N = 90$. The main reason is that in a short knot, the interactions between the monomers are more frequent than in a longer one. As a consequence, the rearrangements such that more monomers of the A type will be in contact with monomers of the B type will lead unavoidably also to contacts between the A and B monomers with themselves. This will increase the energy of the obtained conformation due to the repulsive interactions to which monomers of the same type are subjected.

One additional transition is related to a process analogous to the shrinking taking place at high temperatures in the case of homopolymers in a good solvent. Indeed, since the A monomers are numerous in the case $N_A >> N_B$ and they are subjected to repulsive interactions, we expect that, at high temperatures, the knot will slightly shrink as homopolymers do. This shrinking process causes in homopolymers just a small peak in the heat capacity,

see Fig. 10, right panel, so that in knotted diblock copolymers the effect on the plots of the heat capacity will be limited. However, the shrinking is visible in the plots of the gyration radius.

The general picture presented above fits very well with the results obtained for knots of length $N = 200$. The plots of the specific heat capacity of Fig. 10, left panel, clearly show that the knots with monomer composition $f \sim 0.83$ ($N_A >> N_B$) have much lower peaks than those with $f = 0.50$ ($N_A \sim N_B$). Moreover, the peaks of the specific heat capacity of the knots with $f \sim 0.83$ occur at significantly lower temperatures ($T \leq 0.50$ the first peak and $T \leq 0.70$ the second peak) than the peak of the specific heat capacity of the knots with $f \sim 0.50$ ($T \sim 1.00$). The sharp increase of the gyration radius following the Interestingly, out of all investigated knots $0_1, 3_1, 4_1, 5_1$ and 6_1 with monomer composition $f \sim 0.83$ (the plots of 0_1 and 6_1 are not reported), the second peak has been replaced by a shoulder only in the heat capacity of the knot 5_1.

Let's now discuss the results of the knots with monomer distribution $D_I(100, 100)$. As previously discussed, in this case double peaks and shoulders are absent from the plots of diblock copolymers when $N_A \sim N_B$. The plots with the heat capacities of knots with $D_I(100, 100)$ pointed out in Fig. 10 confirm this expectation. Moreover, the peaks of the specific heat capacity are much higher than those of knots with $D_I(167, 33)$.

The data of longer knots with $N = 300$ and $N = 500$ agree with the previous conclusions, see Figs. 12–14. In longer polymers, a third small peak appears in the case of knot 4_1 with $N = 300$ and monomer distribution $D_I(250, 50)$, see Fig. 13, left panel. As explained before, this extra peak could be related to the presence of a metastable state. In the inset of Fig. 12 it is shown that the rapid growth of the gyration radius at about $T \sim 0.35$ corresponds to the first peak in the specific heat capacity. The middle peak at about $T \sim 0.6$ corresponds to a temperature in which the swelling rate is slowing down considerably, see the inset. We interpret this with the fact that the knot is captured into a metastable state, which stabilises the size of the knot over a small interval of temperatures. One should keep in mind that the detection of metastable states in long knots is particularly difficult. Indeed, there are hints that the energy landscape for long polymers could be funnel-like like in proteins[54]. Thus, long knots are complex systems and the search for metastable states requires an extended sampling before they are found.

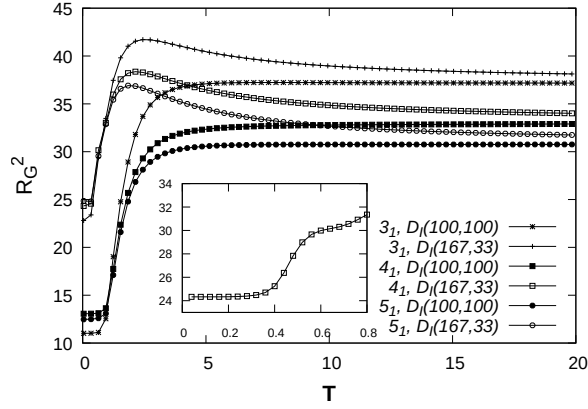Finally, also the data of the gyration radius in the case of polymers with $N = 500$

FIG. 9. Dependence of the mean square gyration radius R_G^2 on the topology and on the monomer composition f in the case of $AB-$diblock copolymers. Presented are the plots of R_G^2 in the case of the knots $3_1, 4_1$ and 5_1 with $N = 200$. For each knots two values of f are considered: $f = 0.50$, corresponding to the monomer distribution $D_I(100, 100)$ and $f \sim 0.83$, corresponding to the monomer distribution $D_I(167, 33)$. In the inset it is shown the detail of the behavior of R_G^2 for the knot 4_1 with monomer distribution $D_I(167, 33)$.
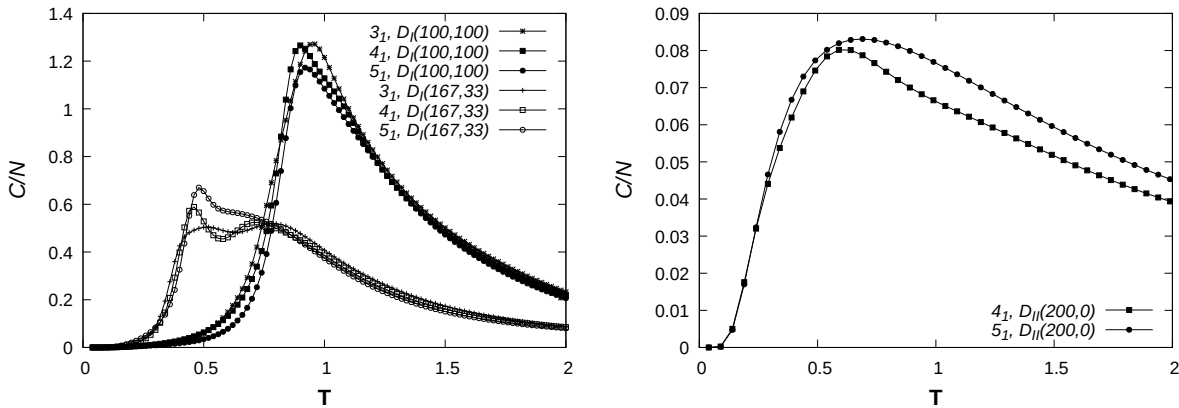
FIG. 10. The left panel shows the dependence of the specific heat capacity C/N on the topology and on the monomer composition f for $AB-$diblock copolymers. The plots of C/N are presented in the case of the knots $3_1, 4_1$ and 5_1 with $N = 200$. For each knot two values of f are considered: $f = 0.50$ (case $D_I(100, 100)$) and $f \sim 0.83$ (case $D_I(167, 33)$). The right panel shows the specific heat capacity of the homopolymer version of the knots 4_1 and 5_1 with $N = 200$ fluctuating in a good solvent.

Knot 4_1, N=200, D_I(167,33), E=-100
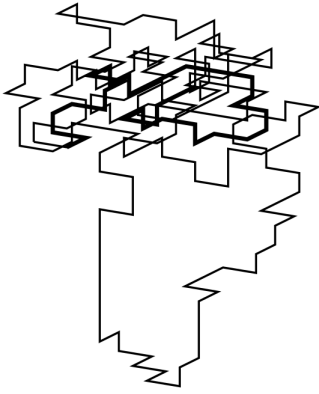
Knot 4_1, N=200, D_I(167,33), E=-105

A-monomers ——
B-monomers ——
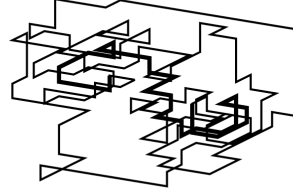
A-monomers ——
B-monomers ——

FIG. 11. This figure shows two sample conformations of a knot 4_1 with length $N = 200$ and monomer distribution $D_I(167, 33)$. The left conformation has energy $E = -100$. It is characterised by a partially ordered portion located in the upper part of the knot in which some of the $A-$monomers are in contact with the $B-$monomers. Other $A-$monomers form a "tail" on the bottom of the knot. At the just slightly higher energy of $E = -105$, the sample conformation of the knot appears very different. The chain containing the $B-$monomers is more stretched than in the case $E = -100$. This allows the formation of two partially ordered portions of the knot concentrated at both ends of the chain with the $B-$monomers. In both pictures the knots have been rescaled in the same way to fit into the page and no different rescaling has been applied to different axes.

confirm the general picture presented before, see Fig. 14. Again, knots with $f \sim 0.50$ ($N_A \sim N_B$) behave differently from those with $f \sim 1$ ($N_A >> N_B$) or, equivalently, $f \sim 0$ ($N_B >> N_A$). As a curiosity, from the performed numerical experiments it turns out that the minimal energy state created by a knot at the lowest temperature is not always the most compact one. Indeed, the size of the knot in two cases (knots 5_1 with monomer distribution $D_I(420, 80)$ and 3_1 with monomer distribution $D_I(400, 100)$) decreases at about $\boldsymbol{T} \sim 0.6$. This is probably due to the excess of monomers of a given type. Indeed, when temperatures are low there are two competing conditions that should be fulfilled in order to minimise the energy. First, the largest possible number of A monomers should be in contact with the few avaliable N_B monomers. At the same time, however, the A monomers cannot get near to each other, as this is energetically expensive due to the repulsive interactions between
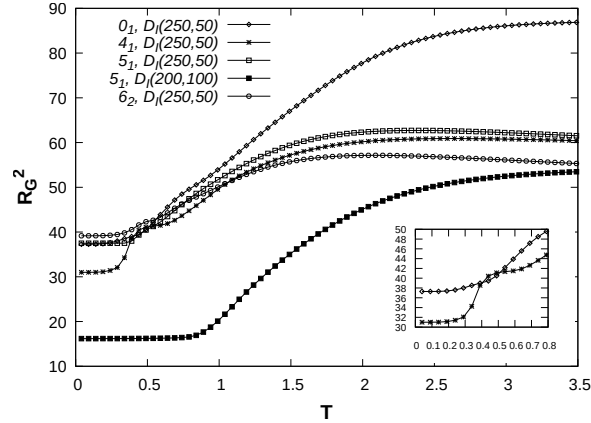
FIG. 12. The data of the gyration radius R_G^2 of knots 0_1, 4_1, 5_1 and 6_2 of length $N = 300$ and monomer distribution $D_I(250, 50)$ are presented. In the case of knot 5_1 it is shown the plot of R_G^2 also for the monomer distribution $D_I(200, 100)$. In the inset the behaviour of the gyration radius of knots 0_1 and 4_1 is displayed in more details at low temperatures. Note the characteristic saddle point in the plot of the gyration radius of knot 4_1 at $\boldsymbol{T} \sim 0.45$.

monomers of equal type. This last requirement is responsible for the fact that the minimal energy state could be not the most compact one. If the temperature is rising, in fact, more energy will be available to the system, so that conformations of the knot in which more A monomers are in contact with themselves become possible. As a consequence, certain knots may attain at higher temperatures a total gyration radius which is smaller than that of the lowest energy state.

To conclude this subsection, we would like to stress that, while homopolymers are simple systems whose size steadily increases (in bad solvents) or decreases (in good solvents) with growing temperatures, diblock copolymers with $f \sim 1$ (or $f \sim 0$), exhibit a more complex behavior. Their mean square gyration radius is smallest at low temperatures and increases up to its maximum value at intermediate temperatures. After that, it starts to decrease and finally stabilizes to some value between the maximum and the minimum at high temperatures. The presence of three different regimes, compact, ultra swollen and swollen is strongly dependent on the monomer composition.
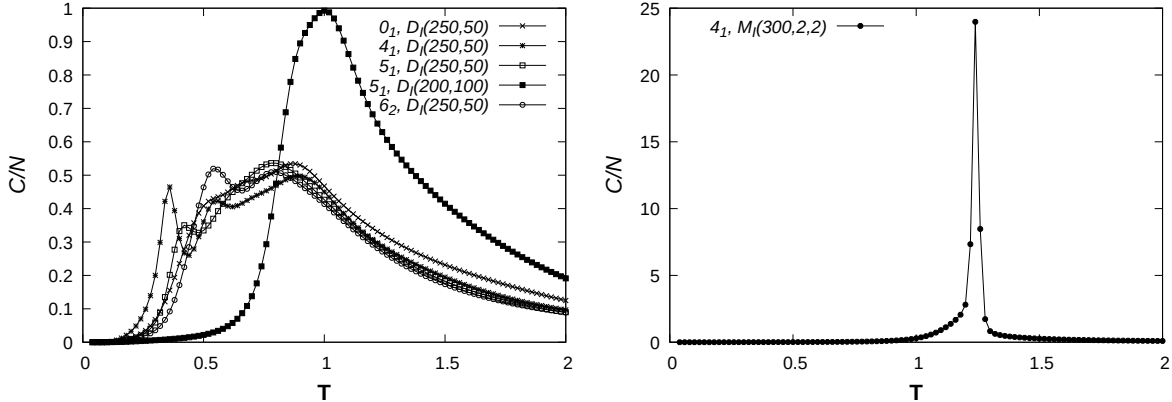
FIG. 13. Left panel: Plots of the specific heat capacity of diblock copolymers with $N = 300$ for knots: 0_1, 4_1, 5_1 and 6_2 with monomer configuration $D_I(250, 50)$. The plot of knot 5_1 with configuration $D_I(200, 100)$ (black squares) has been added to show the differences when the number of monomers of type A and B become comparable. As we see, the specific heat capacity of this knot exhibits just a single peak that is higher than those of the knots with $D_I(250, 50)$. Moreover, the peak appears at a much higher temperature with respect to all other knots in which $N_A = 250$ and $N_B = 50$. The strongest observed compact states have been observed in the case of the monomer distribution $M_I(N, 2, 2)$ (right panel).

B.   Results for Setup II

In Setup II the monomers of type A repel themselves, while monomers of type A and B are subjected to excluded volume forces. Only the monomers of type B attract themselves. For that reason, it could be expected that the behavior of knots in Setup II will be similar to that of the purely repulsive case (i. e. they attain the largest size at very low temperatures to minimize the energy and then shrink upon heating) unless the number N_B of monomers B will be sufficiently high to trigger some behavior typical of attractive interactions (i. e. they swell when heated). This expectation is only partially true. For instance, knots formed by diblock-copolymers with $N_B << N_A$ exhibit a phase of fast, but moderate expansion when heated, so in this sense they share some properties of knots in a bad solvent despite the fact that the monomers of type A subjected to repulsive forces constitute an overwhelming majority. On the contrary, when $N_A = N_B$ the size of the knot does not exhibit any significant change. If instead $N_B >> N_A$, attractive interactions are overwhelming and
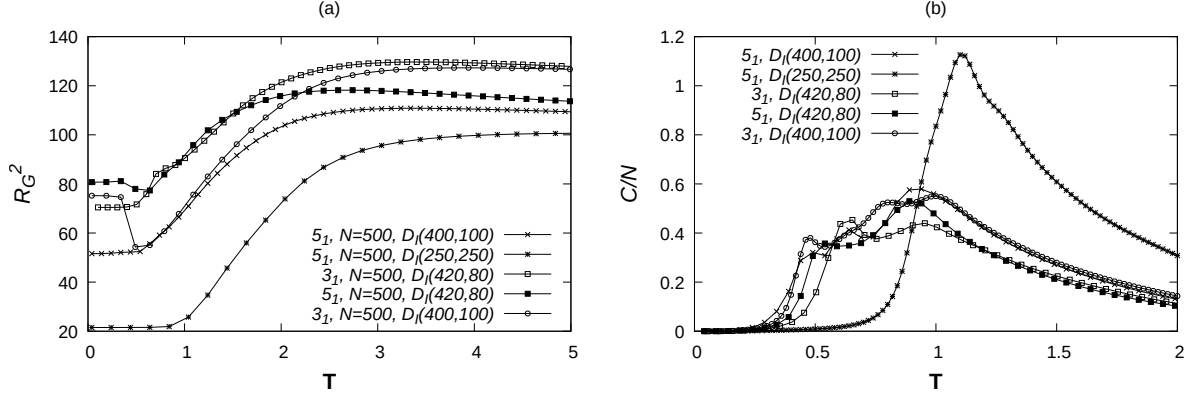
FIG. 14. Plots of the gyration radius (left panel) and specific heat capacity (right panel) of a few knots with length $N = 500$ in three different monomer distributions.
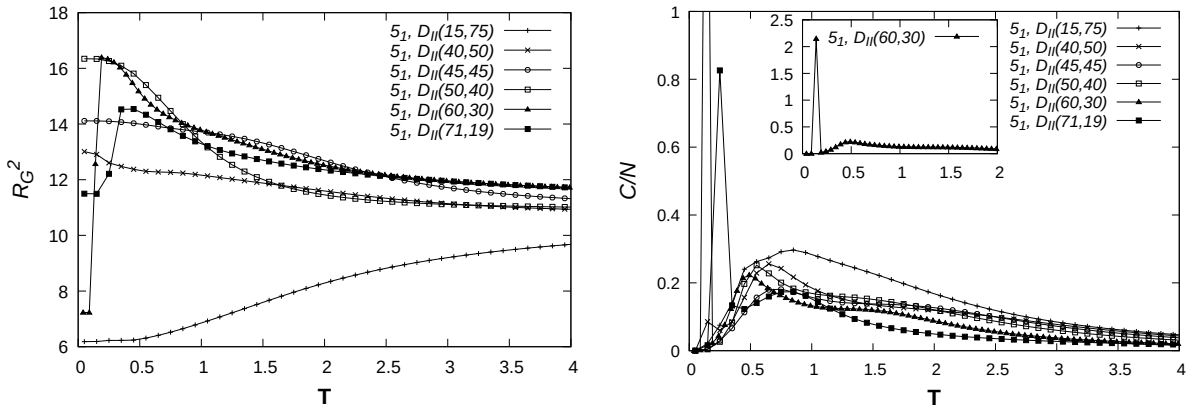

FIG. 15. The mean square gyration radius R_G^2 (left panel) and the heat capacity (right panel) for a knot 5_1 in Setup II with $N = 90$ and different types of monomer distributions.

the behavior of the knot becomes similar to that of a polymer in a bad solvent. In all cases, including the monomer distribution $M_{II}(N, 2, 2)$, the swelling is much less marked than in Setup I. It takes place in a limited range of temperatures and it is soon followed by the shrinking which is typical of homopolymers in a good solvent. The situation is well summarized by Fig. 15 in which the mean square gyration radii and the specific heat capacities of a knot 5_1 of length $N = 90$ are displayed for different monomer distributions. A possible explanation of the different behaviours between the cases $N_A >> N_B$ and $N_A \sim N_B$ is that in the latter case the B monomers form a larger number of contacts. The compact

state that arises in this way is stable under temperature changes and it starts to melt only at high temperatures, i. e. when $T \sim 1.00$ similarly as the powerful compact states built by homopolymers in a bad solvent. At such high temperatures the melting process and the shrinking process are no longer well distinguishable in the plots of the specific heat capacity, while this is possible when the monomer distribution is such that $N_A >> N_B$ and the melting of the compat state takes places at much lower temperatures.

It is worth noticing that in the knot 5_1 the swelling and shrinking phases are well recognizable only when the number of B monomers is small. This is the case of the monomer distributions $D_{II}(71, 19)$ or $D_{II}(60, 30)$, see left panel of Fig. 15. This fact is also visible in the plots of the specific heat capacity of this knot (lines with black squares and black triangles in the right panel of Fig. 15 which are characterised by a double peak. The first peak can be associated to the swelling process with the melting of the compact state formed by the B monomers and the second, at higher temperatures, to the shrinking process. Indeed, the first peaks in the case of the monomer distributions $D_{II}(71, 19)$ and $D_{II}(60, 30)$ are centered more or less at the temperatures in which the swelling phase is taking place. The second peaks are instead much broader and appear in the range of temperatures in which shrinking takes place. Finally, the heights of the peaks are of the expected order, with higher peaks in the case of swelling and lower in the case of shrinking.

To check the effects of topology, in Fig. 17 we have displayed the gyration radii of different knots with two monomer compositions, namely $f = 0.50$ ($D_{II}(45, 45)$ and $f = 0.79$ ($D_{II}(71, 19)$). As it is possible to see, also the knots 3_1 and 4_1 exhibit the same behaviors already observed in Fig. 15 in the case of knot 5_1. However, as a general trend, it turns out that the swelling process taking place in knots with monomer composition $f = 0.79$ becomes increasingly more abrupt and start at lower temperatures with growing topological complexity. This influence of topology is also visible in the plots of C/N of Fig. 18. As a matter of fact, when $f = 0.79$, the heights of the peaks of the specific heat capacity is gradually rising passing from the knot 3_1 to the knot 6_1. Moreover, the temperature around which the peak of C/N is centered is decreasing with increasing knot complexity. We notice in Fig. 18 that knot 4_1 with monomer distribution $M_{II}(90, 2, 2)$ undergoes a swelling process that is much milder than that of the same knot in Setup I.

Going to longer knots, we see in general a fading out of the effects of topology. This is for instance visible in the fact that the knots with monomer distributions $D_{II}(100, 100)$
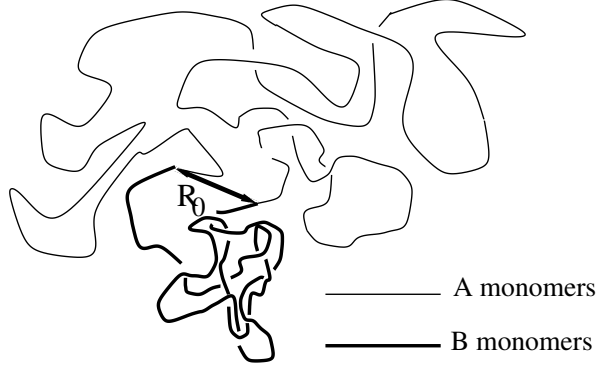
FIG. 16. This figure summarises the situation of knotted diblock copolymers in Setup II: Two chains, one with $A-$type monomers and the other with $B-$type monomers, are attached together at their ends to form a knot. Both chains share the same end-to-end distance $\boldsymbol{R}_0$. It turns out that the equilibrium value of the length $|\boldsymbol{R}_0|$ of $\boldsymbol{R}_0$ is determined not only by the monomer distribution, but also by topology. The A monomers contribute to the increase of $|\boldsymbol{R}_o|$ because they are subjected to repulsive interactions. On the contrary, the B monomers, subjected to attractive interactions, and increasing topological complexities of the knot, both contribute to the decrease of $|\boldsymbol{R}_0|$.

in Fig. 19 have more or less the same behaviour. A remarkable exception is the knot 3_1 with monomer distribution $D_{II}(167, 33)$ whose values of the gyration radius are decidedly greater than those of knots 4_1 and 5_1 with the same monomer distribution. This effect is certainly due to topology and it has been observed also in the case of the knot 3_1 with length $N = 90$ and monomer distribution $D_{II}(60, 30)$. A temptative explanation of this phenomenon can be the following. Looking at the picture in Fig. 16, we see that in Setup II knots consist into two open chains, one with monomers of type A and one with monomers of type B, joined together at their ends. For this reason, the end-to-end distance R_0 is common for both chains. R_0 determines to some extent also the gyration radii of these chains and eventually the gyration radius of the whole knot. Clearly, the segment with the A monomers, which are subjected to repulsive interactions, will try to increase the value of R_0. On the contrary, the segment with the B monomers which are attracting themselves, will tend to have smaller values of its end-to-end distance. If the monomer distribution is $D_{II}(167, 33)$, then the repulsive interactions will certainly be dominating because of the large number of A monomers. This would imply that the value of R_0 will be mainly determined by the part with the A monomers. However, if the topology of the knot is complex, then the numbers
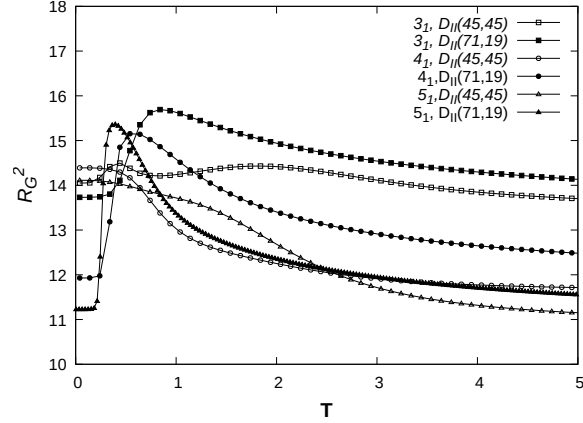
FIG. 17. The mean square gyration radius R_G^2 of knots of different topology and monomer distributions in Setup II. The length of all knots is $N = 90$. The plots with black points (black squares, circles and triangles) correspond to knots with monomer conformations such that $N_A >> N_B$, while those with white points (white squares, circles and triangles) correspond to knots in which $N_A \sim N_B$. In the former case, it is possible to distinguish an expansion of the knot followed by a shrinking phase. When $N_A \sim N_B$, only shrinking is observed or, at most, small size fluctuations (knot 3_1, white squares). There are strong effects of topology that may be easily detected by looking separately at the plots with black and white points.
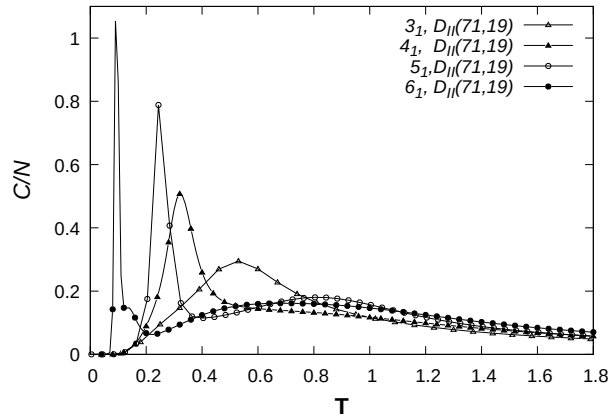

FIG. 18. The specific heat capacity C/N of knots of different types and monomer distributions. The length of all knot is $N = 90$. This picture shows that there are important effects of topology in the behaviour of the knots.
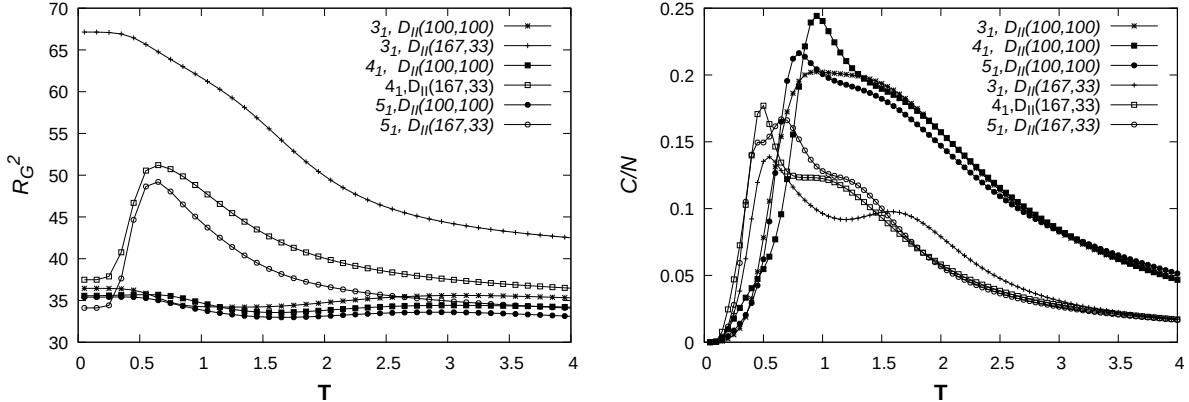
FIG. 19. The mean square gyration radius R_G^2 of knots of different types and monomer distributions. The length of all knots is $N = 200$.

of turns made by the path of the segment with the A monomers will be high. This will make the knot more compact and thus also R_0 will be relatively smaller than in simpler topologies. In this situation it is very likely that the effects of the fluctuations to which the A monomers are subjected will be hampered by the topological constraints and will not be able to destroy the contacts made by the B monomers. If this happens, there is a chance that the the B monomers will prevail and succeed to keep the value of R_0 small as required by the energy and entropy considerations for segment B. As far as it is possible to see from our simulations, this topological mechanism to keep together the knot in a compact state is working when the topology is more complex than that of a knot 3_1.

IV. CONCLUSIONS

The Wang-Landau algorithm has been applied here to study the thermal properties of knotted copolymers in a solution. Two different types of monomers have been considered, called type A and type B. The monomers are subjected to very short-range interactions. Two different setups have been investigated. Setup I corresponds to the case of charged monomers in an ion solution. The A−type monomers carry a positive charge and B−type monomers a negative one. In Setup II the monomers are not charged, but the solvent is good for type A monomers and bad for the B monomers. Block copolymers knots exhibit a more complex behaviour than knotted homopolymers. The latter are in fact simple two-

state systems. When they are in a bad solvent, they are found at very low temperatures in extremely compact and ordered conformations, called crystallites following[55]. With the increasing of the temperature, these knots start to swell until the state of expanded coils is reached. The swelling process is much less violent than in the case of linear polymer chains studied in[55], whose specific heat capacity is characterized by a very sharp peak. In knotted polymer rings, the peak caused by swelling is much broader. When the solvent is good, instead, knots made by homopolymers are in an expanded state at low temperatures and slightly shrink with increasing temperatures, see[47,48].

The introduction of monomers of two kinds drastically changes this situation. For example, for suitable values of the monomer composition f, knots formed by $AB-$diblock copolymers in an ion solution (Setup I) perform as homopolymers in a bad solvent at low temperatures, but exhibit features typical of homopolymers in a good solvent at high temperatures. In practice, they become systems with several states in which at least three different states can be distinguished. At low temperatures these knots are found in the compact and ordered state of crystallites. With growing temperatures, they are swelling like homopolymers in a bad solvent, but after a maximum gyration radius is reached, they start to shrink like knotted homopolymer rings in a good solvent. Examples of this behaviour are in Setup I the knot 3_1 with monomer distribution $D_I(75, 15)$ of Fig. 3 and in Setup II the knot 5_1 with monomer distribution $D_{II}(60, 30)$ of Fig. 15. By choosing the topology and the monomer composition of the knot, it is possible to tune both its size at different temperatures and the temperature at which the maximum value of the gyration radius is attained. Also the range in which the gyration radius is allowed to vary can be determined to some extent. Knots with such features are clearly an advantage with respect to homopolymers in potential medical applications and in the production of intelligent polymer materials containing knots.

In Setup II, knots formed by $AB-$diblock copolymers have a behavior that is strongly dependent on the monomer composition f. Following the intuition, if the number of A monomers largely exceeds that of B monomers, i. e. $N_A >> N_B$, then it could be expected that knots behave like knotted homopolymer rings in a good solvent, since the A monomers are subjected to repulsive interactions. Conversely, if $N_B >> N_A$ and the B monomers are below the theta point, we would rather expect a behavior typical of a homopolymer knot in a bad solvent. The performed simulations show however that the situation is more complicated

than that. For instance, in the case $N_A >> N_B$ we see from Fig. 17 that, in the case of the knots $3_1, 4_1$ and 5_1 with monomer distribution $D_{II}(71, 19)$, the less numerous B monomers play the dominant role at very low temperature. Indeed, these knots exhibit features typical of homopolymers in a bad solvent, i. e. they swell with growing temperatures.

Multiblock copolymers in the classes $M_I(N, n_A, n_B)$ and $M_{II}(N, n_A, n_B)$, where n_A and n_B are small in comparison to N, have remarkable properties too. These properties are not easily predictable by simply looking at the polymer composition. For example, we observe a transition from the compact state to the swollen state which is much more abrupt than that of knots realized using monomers of the same type or diblock copolymers.

The main conclusions of this work can be summarised as follows:

1. The strongest compact states due to the contacts formed by the monomers subjected to attractive interactions have been observed in knots of various lengths with monomer distribution $M_I(N, 2, 2)$, see Figs. 5, right panel and 13, right panel. The specific heat capacity of these knots is characterised by a high peak concentrated in a very narrow range of temperatures corresponding to the melting of these bound states. This interpretation is corroborated by the fact that, exactly in the same range of temperatures, the knot undergoes a sudden and rapid swelling process. When monomer distributions of the kind $M_I(N, n_A, n_B)$ are considered with increasing values of n_A and n_B $(n_A, n_B = 4, 8, ...)$, the peak widens and its height becomes lower, implying that strong compact states are still present at least up to the tested value of $n_A = n_B = 8$, but they become weaker and weaker.

2. Topological effects strongly influence the behaviour of knots in the case of short polymers ($N \sim 90$). Examples of these effects in Setup I can be observed in the plots of the gyration radius and specific heat capacity reported in Fig. 7 and in Fig. 8 respectively. Fig. 18 displays the changes due to topology of the heights and temperatures of the peaks of the specific heat capacity in the case of Setup II. With increasing polymer lengths these effects fade out and the choice of the monomer distribution becomes the main factor influencing the properties of the knots. Yet, topology is still relevant for longer polymers because it provides a way to fine tune their behaviour. For instance, the effects of topology when $N = 200$ on the way in which the gyration radius changes with different temperatures are reported in Fig. 9. A certain dependence on topology

of the heights of the peaks of the specific heat capacity can also be spotted in the plots of Fig. 10 where knots of length $N = 200$ are considered. However, in general the influence of topology is more visible in the plots of the gyration radius. Let us notice that topology plays some role even in the case of the longest polymers that have been investigated here. For instance, the knot 3_1 with $N = 500$ and monomer distribution $D_I(400, 100)$ is suddenly shrinking at a temperature of $\boldsymbol{T} \sim 0.5$ (the value of R_G^2 goes from 75 to 52), a feature that is not so marked in the case of the other knots whose plots have been displayed in Fig. 14, left panel, including the knot 5_1 with the same monomer distribution.

3. Several exceptions to the rule that the influence of topology should fade out with increasing polymer lengths have been observed. For instance, the gyration radius of the knot 3_1 with length $N = 200$ and monomer distribution $D_{II}(167, 33)$ is much larger than the gyration radii of knots 4_1 and 5_1 with the same lengths and monomer distribution, see Fig. 19. This striking difference can be explained by the strong entropic effects induced in Setup II by the fact that the paths of the knots are subjected to topological constraints, see Fig 16 and related comments. Also when $N = 90$, it is possible to see from Fig. 17 that, when the monomer distribution is $D_{II}(71, 19)$, the swelling of the knot 3_1 with rising temperatures is much more limited than that of knots 4_1 and 5_1.

4. A characteristics that emerges in knotted block copolymers and is not present in the case of homopolymers, is the existence of rearrangements of the knot structures at low temperature. In some cases, this leads to intermediate states. These rearrangements can be detected by the appearance of extra peaks or shoulders in the specific heat capacity of longer knots in Setup I. Metastable intermediate states have been observed for instance in knot 3_1 with $N = 500$ and monomer distribution $D_I(400, 100)$, see Fig. 14, right panel, and knot 4_1 with $N = 300$ and monomer distribution $D_I(250, 50)$, see Fig. 13.

The simulations presented in this paper require the sampling of an extensive amount of knot conformations. Despite major improvements in the sampling procedure, that of rare events is still a problem in the case of very long polymers. Some of the conformations appear after several hundred billions of trials and their inclusion extends enormously the

calculation times. Moreover, in this work very short-range interactions have been considered. This is enough to study the cases of flexible knots in a good or bad solutions, but it would be interesting to add more complicated interactions. In this way it would be possible to consider for instance also the polymer rigidity and the transition from bad to good solvents at the theta point. Work is in progress to implement in our code the backbone rigidity and the Lennard-Jones interactions.

ACKNOWLEDGMENTS

---

[*] neda.abbasi_taklimi@phd.usz.edu.pl

[†] franco@feynman.fiz.univ.szczecin.pl

[‡] marcin.piatek@usz.edu.pl

[§] luca.tubiana@unitn.it

[1] *Molecular Catenanes, Rotaxanes and Knots, A Journey Through the World of Molecular Topology*, J. P. Sauvage, C. Dietrich-Buchecker (Eds.), (Wiley-VCH Verlag, Weinheim, 1999).

[2] J. Arsuaga, J. Roca and D. W. Sumners, *Topology of viral DNA*, in *Emerging Topics in Physical Virology* , P. G Stockley and R. Twarock (Eds.), (Imperial College Press, London, 2010).

[3] G. Gil-Ramirez, D. A. Leigh and A. J. Stephens, *Catenanes: Fifty Years of Molecular Links*, *Angewandte Chemie International Edition* **54** (21) (2015), 6110.

[4] J.-P. Sauvage and D. B. Amabilino. *Templated synthesis of knots and ravels*, in *Supramolecular Chemistry: From Molecules to Nanomaterials*, P. A. Gale and J. W. Steed (Eds.), (Wiley Online Library, 2012).

⁵ *Topological Polymer Chemistry*, Y. Tezuka (Ed.), (World Scientific, Singapore, 2013).

⁶ S. D. P. Fielden, D. A. Leigh and S. L. Woltering, *Angew. Chem. Int. Ed.* **56** (37) (2017), 11166.

⁷ M.-L. Tong and X.-M. Chen, *Chapter 8 - Synthesis of Coordination Compounds and Coordination Polymers*, in *Modern Inorganic Synthetic Chemistry (Second Edition)*, Ruren Xu and Yan Xu (Eds.), (Elsevier B. V., 2017), pp 189-217.

⁸ T. Stauch and A. Dreuw, *Angewandte Chemie International Edition* **55** (2) (2016), pp.811-814.

⁹ N. Katsonis, F. Lancia, D. A. Leigh, L. Pirvu, A. Ryabchun and F. Schaufelberger, *Nature Chemistry* (2020), pp.1-6.

¹⁰ U. Tkalec, M. Ravnik, S. Čopar, S. Žumer and I. Muševič, *Science*, **333**(6038) (2011), pp.62-65.

¹¹ L. H. Kauffman, *Knots and Physics* (Vol. 1) (2001), World Scientific.

¹² L.H. Kauffman, S. Lambropoulou, Classifying and applying rational knots and rational tangles. Physical Knots: Knotting, Linking and Folding Geometric Objects, J.A. Calvo, K.C. Millett, E.J. Rawdon, Eds.; Contemporary Mathematics AMS Series 304, (2002), pp. 223-258.

¹³ A. Y. Grosberg, *Polym. Sci. Ser.* **A 51** (2009), 70–79.

¹⁴ A. Suma, A. Rosa and C. Micheletti, *ACS Macro Letters* **4** (12) (2015), 1420-1424.

¹⁵ L. Tubiana, E. Orlandini, C. Micheletti, *Progress of Theoretical Physics Supplement* **191** (2011), 192-204.

¹⁶ A.L. Kholodenko, T.A. Vilgis, Physics Reports, **298**, (5–6) (1998), 251-370.

¹⁷ S. Majumder, M, Marenz, S, Paul, and W. Janke, *Macromolecules* **54** (12) (2021), 5321-5334.

¹⁸ E. Orlandini, M. Baiesi and F. Zonta, *Macromolecules*, **49** (12) (2016), 4656.

¹⁹ L. Dai and P. S. Doyle, *Polymers* **9**(2) 2017, p.57.

²⁰ C. Vlahos, N. Hadjichristidis, M. K. Kosmas, A. M. Rubio and J. J. Freire, *Macromolecules* **28** (1995), 6854.

²¹ J.F. Marko, *Macromolecules* **26** (6) (1993), pp.1442-1444.

²² A. Weyersberg and T. A. Vilgis, *Phys. Rev. E* **48** (1) (1993), 377.

²³ R. Hołyst and T. A. Vilgis, *Macromolecular theory and simulations* **5**(4) (1996), pp.573-643.

²⁴ K. Huber, *Macromolecules* **21** (5) (1988), 1305.

²⁵ R. H. Abdolvahab, M. R. Ejtehadi, and R. Metzler, *Physical Review E* **83**(1), p.011902.

²⁶ N. A. Volkov, P.N. Vorontsov-Velyaminov, and A. P. Lyubartsev, *Physical Review E* **75** (1) (2007), p.016705.

²⁷ K. A. Dill, S. Bromberg, K. Yue, K. M. Fiebig, D. P. Yee, P. D. Thomas,and H. S. Chan, **RE-**

VIEW *Principles of protein folding - A perspective from simple exact models*. Protein Science, 4:561-602. Cambridge University Press, 1995.

[28] T. Wüst, D. P. Landau, *J. Chem. Phys.* **137** (2012), 064903.

[29] T. Wüst, D. Reith, and P. Virnau, *Phys. Rev. Lett.* **114** (2) (2015), 028102.

[30] S. Najafi, R. Potestio, *PLoS ONE* **10** (7) (2015), e0132132.

[31] A. Kuriata and A. Sikorski, *Macromolecular Theory and Simulations* **27** (2018), 1700089.

[32] H. Benahmed, *Chinese Journal of Physics* **73** (2021), pp.256-274.

[33] A. Tagliabue, C. Micheletti and M. Mella, *ACS Macro Letters* **10**(11) 2021, pp.1365-1370.

[34] T. Herschberg, J.-M. Y. Carrillo, B. G. Sumpter, E. Panagiotou, and R. Kumar *Macromolecules* **54** (16) (2021), 7492-7499.

[35] C. Cardelli, L. Tubiana, V. Bianco, F. Nerattini, C. Dellago, and I. Coluzza, *Macromolecules* **51** (21) (2018), 8346–8356.

[36] F. Wang and D. P. Landau, Phys. Rev. Lett. 86 (2001), 2050.

[37] W. Wang, Y. Li and Z. Lu, *Science China Chem.* **58** (9) (2015), 1471.

[38] A. Swetnam, C. Brett and M. P. Allen, *Phys. Rev. E* 85 (2012), 031804.

[39] F. Ferrari, *Block copolymer knots*, arXiv:1603.08972[cond-mat.soft] (2016).

[40] Junhwan Jeon and Andrey V. Dobrynin, *J. Phys. Chem. B* **110** (2006), 24652.

[41] Ying Wai Li et al, *J. Phys.: Conf. Ser.* **510** (2014), 012012.

[42] E. E. Borrero, and C. Dellago, *Jour. Chem. Phys.*, **133**(13) (2010), p.134112.

[43] Y. W. Li, T. Vogel, T. Wüst, and D. P. Landau, *Journal of Physics: Conference Series* **510** (1) (2014), p. 012012.

[44] Y. Zhao and F. Ferrari, *Physica A: Statistical Mechanics and its Applications*, **486** (2017), 44-64.

[45] E. J. Janse van Rensburg and A. Rechnitzer, *J. Stat. Mech.* (2011), P09008.

[46] R. Scharein et al, *J. Phys. A: Math. Theor.* **42** (2009), 475006.

[47] Y. Zhao and F. Ferrari, JSTAT *J. Stat. Mech.* (2012), P11022.

[48] Y. Zhao and F. ferrari, J. Stat. Mech. (2013), P10010.

[49] N. Madras, A. Orlistsky and L. A. Shepp, Journal of Statistical Physics 58, 159 (1990).

[50] F. Rampf, W. Paul, and K. Binder, *Europhys. Lett.* bf 70 (2005), 628.

[51] T. Vogel, M. Bachmann and W. Janke, *Phys. Rev. E* **76** (2007), 061803.

[52] M. Bachmann and W. Janke, *Phys. Rev. Lett.* **91** (2003), 208105.

[53] Y.-H. Hsieh, C.-N.Chen and C.-K. Hu, *EPJ Web of Conferences* **108** (2016), 01005.

[54] F. Ferrari and Y. Zhao, *Reviews in Mathematical Physics* **33** (02) (2021), 2150005.

[55] M. P. Taylor, W. Paul and K. Binder, *The Journal of chemical physics*, **131**(11) (2009), p.114907.

[56] Let us note that in the present case the knot has length $N = 90$. Due to the fact that 90 is not divisible by four, the monomer sequence is obtained by joining together $\nu = 22$ basic units of the kind $AABB$ and putting at the end of the sequence (monomers 89 and 90) two monomers of the A type. As a consequence, the sequence looks as follows: $AABB - AABB - \cdots - AABB - AA$.